

ONIOM Study of the Mechanism of the Enzymatic Hydrolysis of Biodegradable Plastics

Yoshitake Sakae,[1] Toshiaki Matsubara,*[1] Misako Aida,[1] Hidemasa Kondo,[2] Kazuo Masaki,[3] and Haruyuki Iefuji[3]

[1]Center for Quantum Life Sciences and Graduate School of Science, Hiroshima University, 1-3-1 Kagamiyama, Higashi-Hiroshima 739-8530

[2]Functional Protein Research Group, Research Institute of Genome-based Biofactory, National Institute of Advanced Industrial Science and Technology, 2-17-2-1 Tsukisamu-Higashi, Toyohira, Sapporo 062-8517

[3]National Research Institute of Brewing, 3-7-1 Kagamiyama, Higashi-Hiroshima 739-0046

Received August 19, 2008; E-mail: matsu05@hiroshima-u.ac.jp

A cutinase-like enzyme (CLE), which is purified experimentally from the yeast *Cryptococcus* sp. strain S-2, has been recently found to degrade biodegradable plastics very efficiently. In this study, we theoretically examine the mechanism of hydrolysis of biodegradable plastics by the CLE by means of the ONIOM method. We optimize all the intermediates and the transition states involved in the considered enzymatic reaction and determine the energy surface of the entire catalytic cycle. The calculations show that the amino acid residues inside the pocket of the active site, Thr17 and Gln86, which stabilize the tetrahedral intermediates, and Gly115 in addition to Ser85, His180, and Asp165, which compose the catalytic triad, significantly contribute to the catalytic reaction. This is similar to the case of serine protease reported to date. Moreover, we have newly found that the energy barrier of the catalytic cycle is significantly lowered by the electronic effect of the OH group in the side-chain of Thr17 and bound water. The calculated potential energy surface of the reaction shows that the cleavage of the ester bond is a rate-determining step.

The natural environment faces a crisis due to the pollution caused by the disposal of plastics. The environmental pollution by plastics becomes more serious year after year. Therefore, biodegradable plastics that can be decomposed to water and carbon dioxide by enzymes in microorganisms widely distributed in nature have attracted much attention as "Green Plastics." In order to utilize these "Green Plastics" more effectively, biological chemists have started to explore more high-performance enzymes.

Recently, Masaki et al. found that an enzyme, which is purified from the yeast *Cryptococcus* sp. strain S-2, exhibits high degradation activity for various biodegradable plastics.[1] Homology analysis of the protein sequence revealed that it is a cutinase-like enzyme (CLE). As shown by the X-ray structure, which is registered in the protein data bank (PDB) with an ID code of 2CZQ,[1] the CLE has three important amino acid residues, Ser85, His180, and Asp165, in the active site as displayed in Figure 1. These three amino acid residues are known as the catalytic triad in the serine protease, which facilitate the catalytic reaction.[2,3] The CLE also has Thr17 and Gln86 in the active site, which will stabilize the large negative charge appearing on the carbonyl oxygen of the substrate in the tetrahedral intermediates, **2** and **5**. The hydrolysis of biodegradable plastics by the CLE would therefore proceed by a reaction mechanism similar to that proposed for the hydrolysis of peptide bonds by serine protease. The mechanism of the hydrolysis of biodegradable plastics by the CLE proposed on the basis of the most commonly accepted mechanism for the hydrolysis of peptide bonds by serine protease[2] is presented in Figure 1.

For serine protease, it is the general consensus that the reaction proceeds via tetrahedral intermediates **2** and **5**, which are stable in energy. The catalytic cycle consists of two reaction processes, i.e., acylation (**1** → **2** → **3**) and deacylation (**4** → **5** → **6**). In the first process, acylation, the incoming substrate (e.g., poly(lactic acid), poly(butylene succinate), and poly(ε-caprolactone)) binds at the active site to form enzyme–substrate complex **1**. In the first step, **1** → **2**, the nucleophilic attack of Ser85 to the carbonyl carbon of the substrate forms a tetrahedral intermediate **2**, where the OH hydrogen of Ser85 migrates to His180 as a proton, and the increased negative charge of the carbonyl oxygen of the substrate is stabilized in energy by the H-bonds contributed by two NH groups of Gln86 and Thr17. In the subsequent step, **2** → **3**, the C–O(R1) bond of the substrate is broken and the R1OH product is formed with the migration of the proton from His180.

The second process, deacylation, starts from the acyl–enzyme complex **4**. In the first step, **4** → **5**, the tetrahedral intermediate **5** is formed by nucleophilic attack of an incoming H_2O molecule. One hydrogen from the H_2O molecule migrates to His180 as a proton and the increased negative charge on the carbonyl oxygen of the substrate is stabilized by the H-bonds contributed by Gln86 and Thr17. In the last step, **5** → **6**, the other product R2(CO)OH is formed by the cleavage of the C–O(Ser85) bond, and the proton on His180 is abstracted by Ser85.

Published on the web March 12, 2009; doi:10.1246/bcsj.82.338

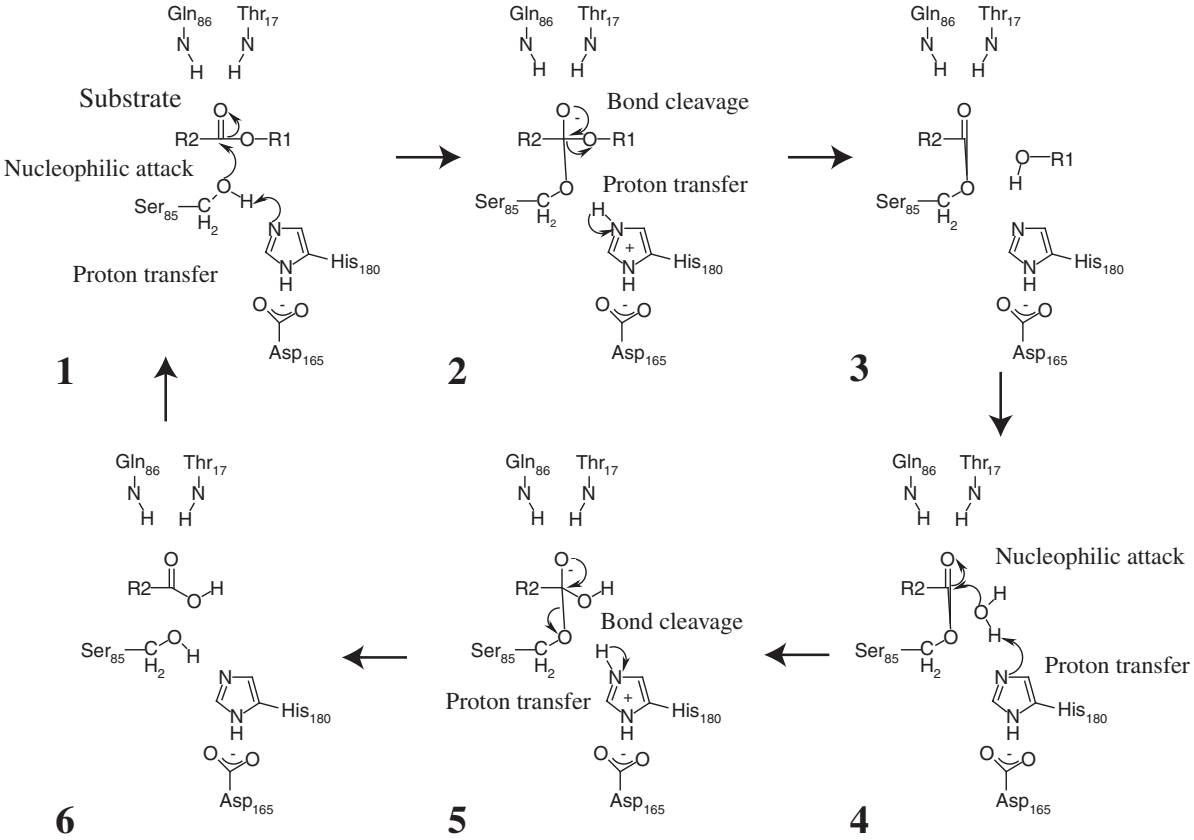

Figure 1. Proposed catalytic cycle for the hydrolysis of biodegradable plastics by the cutinase-like enzyme (CLE) on the basis of the most commonly accepted catalytic cycle for the hydrolysis of the peptide bond by serine protease.

According to this mechanism, we theoretically examined the hydrolysis of biodegradable plastics by the CLE by means of the ONIOM method. The catalytic cycle that passes through the tetrahedral intermediates, **2** and **5**, seems to be quite reasonable, because the large negative charge formed on the carbonyl oxygen of the substrate in **2** and **5** is stabilized in energy by the amino acid residues, Gln86 and Thr17. As we already know for serine protease, the catalytic triad consisting of Ser85, His180, and Asp165, will form a H-bond network. The H atom would shift as a proton from Ser85 to His180 through this H-bond network in the step **1** → **2** to enhance the nucleophilicity of the OH oxygen of Ser85 and develop a negative charge on the carbonyl oxygen of the substrate. The mechanism of the net transfer of the proton in the catalytic triad, i.e., single or double proton transfer, is still under debate for serine protease.[4–10] In the case of the double proton transfer, the H atom on His180 also shifts to Asp165 as a proton. A similar net transfer of the proton is also expected in the step **4** → **5**. We can thus intuitionally predict that the neighboring amino acid residues, Gln86, Thr17, Ser85, His180, and Asp165, play an important role to lower the energy barrier of the nucleophilic attack in the steps, **1** → **2** and **4** → **5**.

We examined the reaction mechanism especially with a focus on the role of the amino acid residues at the active site. We optimized the intermediates and transition states and determined the potential energy surface of the entire catalytic cycle using a realistic model of the enzyme obtained from the crystal structure of the CLE and a model substrate. As a result, it was found that the energy barrier of the catalytic cycle is lowered by an electronic effect of the OH group of the side-chain of Thr17. It was also discovered that bound water in the active site significantly contributes to the reaction.

Computational Details

The initial structure of the cutinase-like enzyme (CLE) was obtained from the crystal structure registered in the protein data bank (PDB) with ID code 2CZQ.[1] The missing hydrogen atoms were added using the TINKER Ver. 4.2 program[11–16] and the added H atoms were optimized with AMBER96 force field parameters[17–21] to get a realistic model of the enzyme. For the substrate, we used $CH_3(CO)OCH_3$ as a model.

We adopted a two-layered ONIOM methodology for the ONIOM[22–28] calculations. Here, the entire system is partitioned into inner and outer layers, which are treated by QM and MM methods, respectively. The inner layer of the QM portion is presented in Figure 2. The side chain of Ser85, His180, and Asp165 forming a catalytic triad and the side and main chain of Gln86 and Thr17 interacting with the substrate are included in the QM. We also included in the QM the portion of the main chain of Gly115, Gly166, and the OH group of the side chain of Tyr183, which would affect the function of His180 as a proton receptor. The hydrogen atoms circled by dotted line are replaced by the corresponding C or N atom in the real system.

All the ONIOM calculations were carried out using the Gaussian03 program package.[29] The QM calculations were performed by the B3LYP method, which consists of a hybrid

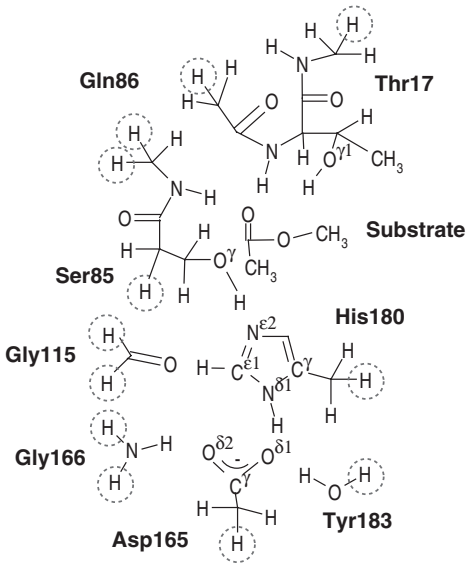

Figure 2. QM part of the active site of the cutinase-like enzyme (CLE) with the substrate. The atoms circled by the dotted line are replaced by H atoms to form the QM part of the ONIOM method.

Becke + Hartree–Fock exchange and a Lee–Yang–Parr correlation functional with non-local corrections.[30,31] The basis set of 6-31G** was used for all the atoms. The MM part was calculated with the AMBER96 force field.[17–21] The generalized AMBER force field (GAFF)[32] parameters were used for the substrate. In order to avoid structural deformation of the entire enzyme, the position of all atoms of the MM portion was frozen in the geometry optimizations. The transition states were determined by a plot of the potential energy versus the reaction coordinate. In the search of each transition state, the length of the C–O bond most significantly related to the reaction was varied with an interval of 0.1 Å. We also performed calculations for the QM subsystem of Model T at the MP2 and B3LYP levels and confirmed that there is no significant difference in the tendency in both geometry and energy between the two levels.

Since the crystal structure of the CLE shows that the active site has a space to provide for bound water, we added one H_2O molecule to the active site and examined the contribution of bound water to the catalytic reaction. We calculated two models of the CLE with bound water, since bound water can contribute to the reaction in two different ways. We also calculated another CLE assuming a mutant, where Thr17 is replaced by Ala17 without the OH group in the side-chain, to reveal the effects of the OH group of Thr17 in the reaction. In the case of a mutant with Ala17, bound water contributes to the reaction in one way. We therefore calculated five models; Model T for Thr17 without, Model TW1 and TW2 for Thr17 with, Model A for Ala17 without, and Model AW for Ala17 with bound water. We added T, TW1, TW2, A, and AW as prefixes to the labels of the intermediates and transition states to distinguish the models.

Results and Discussion

Model T. The catalytic reaction undergoes two processes as mentioned above, namely, acylation (**T-1** → **T-TS1** → **T-2** → **T-TS2** → **T-3**) and deacylation (**T-4** → **T-TS3** → **T-5** → **T-TS4** → **T-6**), as presented in Figure 3. In the starting enzyme–substrate complex **T-1**, two N–H groups of the main chain of Thr17 and Gln86 form the H-bonds with the carbonyl oxygen of the substrate with N···H distances of 1.898 and 2.161 Å. In addition, the OH group of the side chain of Thr17 also forms a H-bond with the carbonyl oxygen of the substrate with a short distance of 1.754 Å. The third H-bond of the OH group of the side chain of the amino acid residues has been similarly reported in subtillisin.[33,34] The OH oxygen of Ser85 stays far from the carbonyl carbon of the substrate with a C···O distance of 2.412 Å. The OH group forms a H-bond with the N of His180 as shown by the H···N distance of 1.593 Å. On the other hand, one of the $-COO^-$ oxygen of Asp165 interacts with the NH hydrogen of His180 with a short distance of 1.693 Å through the H-bond. Due to this strong electrostatic interaction, the N–H distance of His180 is stretched to 1.048 Å. Thus, the catalytic triad consisting of Ser85, His180, and Asp165 is formed by H-bonds.

In the transition state of the nucleophilic attack of Ser85 to the substrate **T-TS1**, the O···C distance is shortened to 1.900 Å and the OH distance is stretched to 1.084 Å. The nucleophilicity of the O is enhanced by the stretch of the OH distance, as shown by its negative charge increased to −0.24 e. In the formed tetrahedral intermediate **T-2**, the H(Ser85) is completely transferred to His180 as a proton and the C–O(Ser85) bond is formed. The carbonyl bond of the substrate is hence stretched to 1.312 Å and the negative charge on the carbonyl oxygen is increased to −0.45 e. Due to the large negative charge on the O, three O···H distances are shortened to 1.844, 1.795, and 1.786 Å. In other words, the NH groups of the main chain and the OH group of the side chain of Gln86 and Thr17 play an important role to stabilize the large negative charge formed on the O. In fact, without these three H-bonds, the potential energy surface of the reaction from **T-1** to **T-2** through **T-TS1** becomes uphill.

On the other hand, the positively charged His180 is stabilized in energy by the interaction with Asp165 and Gly115. The H-bond between the $C^{\varepsilon 1}H$ of the imidazole ring of His with the neighboring amino acid residue has been previously reported for serine hydrolases.[35–37] Both H···O(Gly115) and H···O(Asp165) interactions are strengthened in **T-2** as shown by their distances shortened to 2.169 and 1.547 Å. Here, it should be noted that the $N^{\delta 1}H$ hydrogen of His180 is not transferred to Asp165, although the $N^{\delta 1}$–H distance of His180 is stretched to 1.083 Å. This result shows that the nucleophilic attack of Ser85 proceeds with a single-proton-transfer mechanism. This is similar to the previous result for serine protease.[37,38] The electrostatic interaction of Tyr183 and Gly166 with Asp165 prevents the transfer of the $N^{\delta 1}H$ hydrogen of His180 to Asp165. We confirmed that the $N^{\delta 1}H$ hydrogen is transferred from His180 to Asp165 without Tyr183 and Gly166. However, it is obvious that the catalytic triad functions to promote the nucleophilic attack of the OH oxygen of Ser85 through the H-bond network. The subsequent reaction starting from the intermediate **T-2** is a cleavage of the C–O bond of the substrate. After passing through the transition state **T-TS2**, the formed CH_3O^- abstracts the proton from His180. By this proton migration, distances of both H-bonds, H···O(Gly115) and H···O(Asp165), are weakened again as

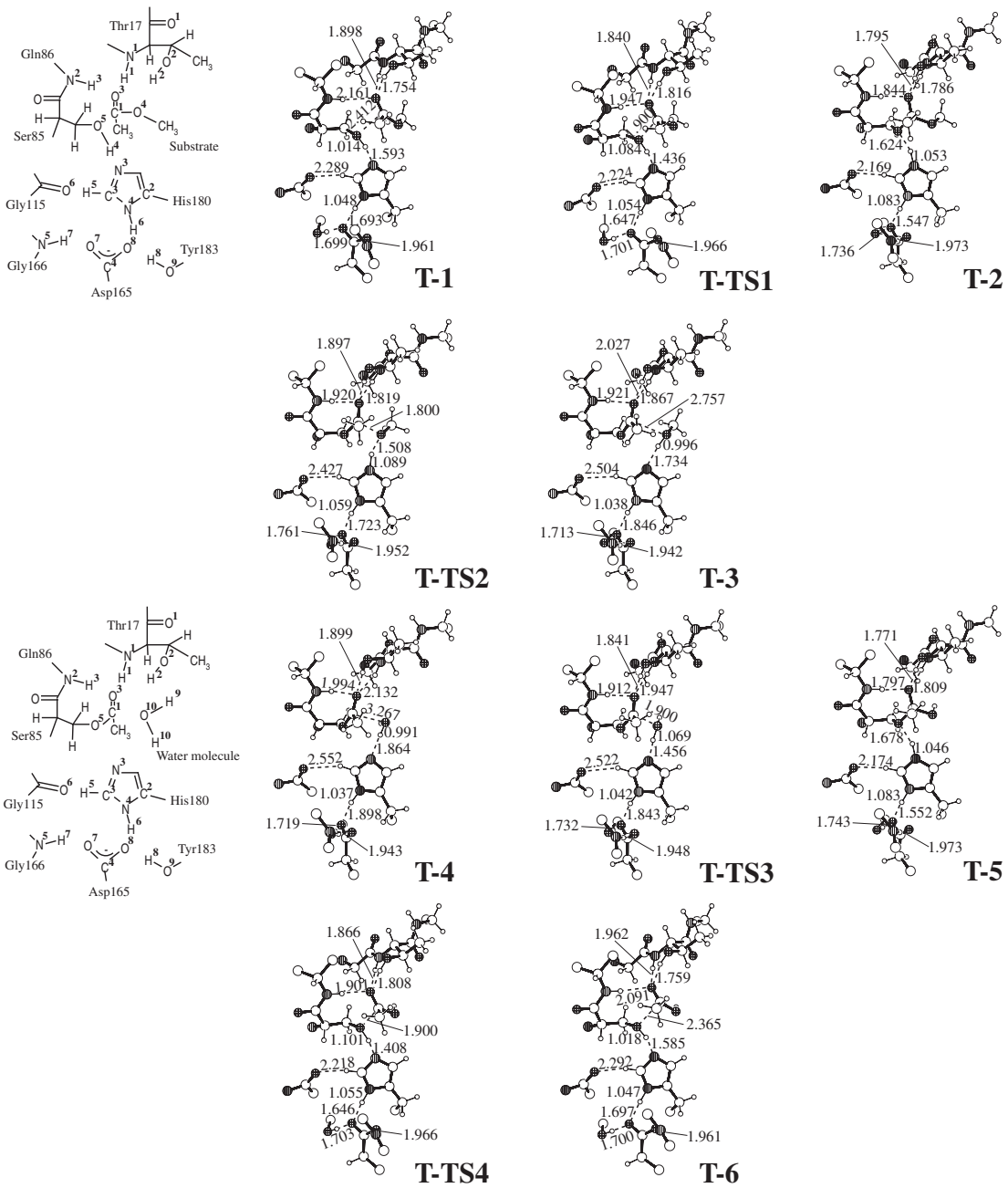

Figure 3. Optimized equilibrium and transition-state structures (in Å) involved in the catalytic cycle of the hydrolysis of biodegradable plastics by the cutinase-like enzyme (CLE) at the ONIOM(B3LYP/6-31G**:AMBER) level for Model T. Only the QM part is displayed for clarity.

shown by their distances of 2.504 and 1.846 Å in **T-3**. The H-bonds between the carbonyl oxygen of the substrate and the amino acid residues, Thr17 and Gln86, are also weakened due to the decrease in the negative charge of the carbonyl oxygen.

The second process of the catalytic cycle, deacylation, starts from the intermediate **T-4**, where the produced CH_3OH is replaced by a H_2O molecule. In the first step, the H_2O oxygen attacks the carbonyl carbon of the substrate to form the tetrahedral intermediate **T-5** through the transition state **T-TS3**. Although the carbonyl bond of the substrate is stretched and the negative charge of the carbonyl oxygen is increased by this attack, it is stabilized in energy by three H-bonds with Thr17 and Gln86. These three H-bonds are gradually strengthened as the reaction proceeds from **T-4** to **T-5**. On the other hand, they are weakened in the second step of the cleavage of the C–O(Ser85) bond, **T-5** → **T-TS4** → **T-6**, since the negative charge on the carbonyl oxygen of the substrate decreases. These trends are the same as those shown in the first process of the catalytic cycle, acylation. Here, among three H-bonds, the O···H(Thr17,OH) distance is the shortest throughout the reaction.

The proton migration within the catalytic triad also shows a tendency similar to that found in the first process, acylation. One of hydrogens of the incoming H_2O is transferred to His180

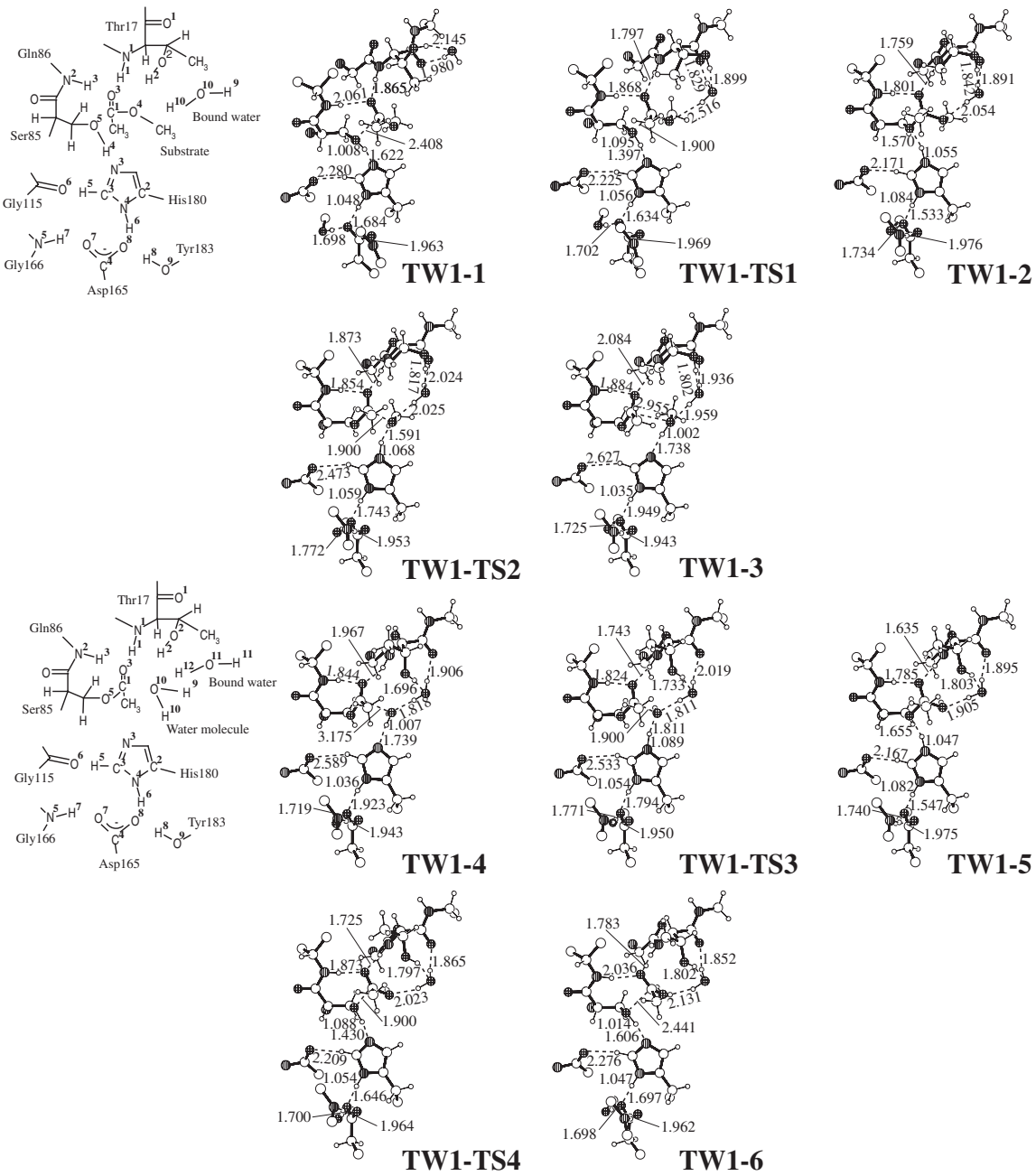

Figure 4. Optimized equilibrium and transition-state structures (in Å) involved in the catalytic cycle of the hydrolysis of biodegradable plastics by the cutinase-like enzyme (CLE) at the ONIOM(B3LYP/6-31G**:AMBER) level for Model TW1. Only the QM part is displayed for clarity.

while the $N^{\delta 1}H$ hydrogen of His180 stays as it is without migration in **T-5**, which shows a single-proton-transfer mechanism. However, the $N^{\delta 1}$–H distance of His180 in **T-5** is stretched to 1.083 Å. On the other hand, the H···O(Gly115) and H···O(Asp165) distances become shortest in **T-5** to stabilize in energy the positively charged His180. In the second step, the proton on His180 is already transferred to Ser85 in the transition state **T-TS4**. The other product $CH_3(CO)OH$ is separated away from Ser85 by this migration of the proton from His180 to Ser85. Thus, the support of the catalytic triad and the OH and NH groups of Thr17 and Gln86 are essential to the catalytic reaction.

Models TW1 and TW2. Since the pocket of the active site of the CLE has enough space for bound water between Thr17 and substrate, we added bound water in this site and examined the contribution to the catalytic reaction. We found two models of interaction of bound water at the active site, which are referred to as Models TW1 and TW2 below. In Model TW1, the bound water interacts with the carbonyl oxygen of the main chain and the OH hydrogen of the side chain of Thr17. It also interacts with the –C–O–C– oxygen of the substrate and bridges Thr17 and the substrate in the first process of the catalytic cycle as presented in Figure 4. In the starting complex **TW1-1**, the bound water does not interact with the substrate. However, one

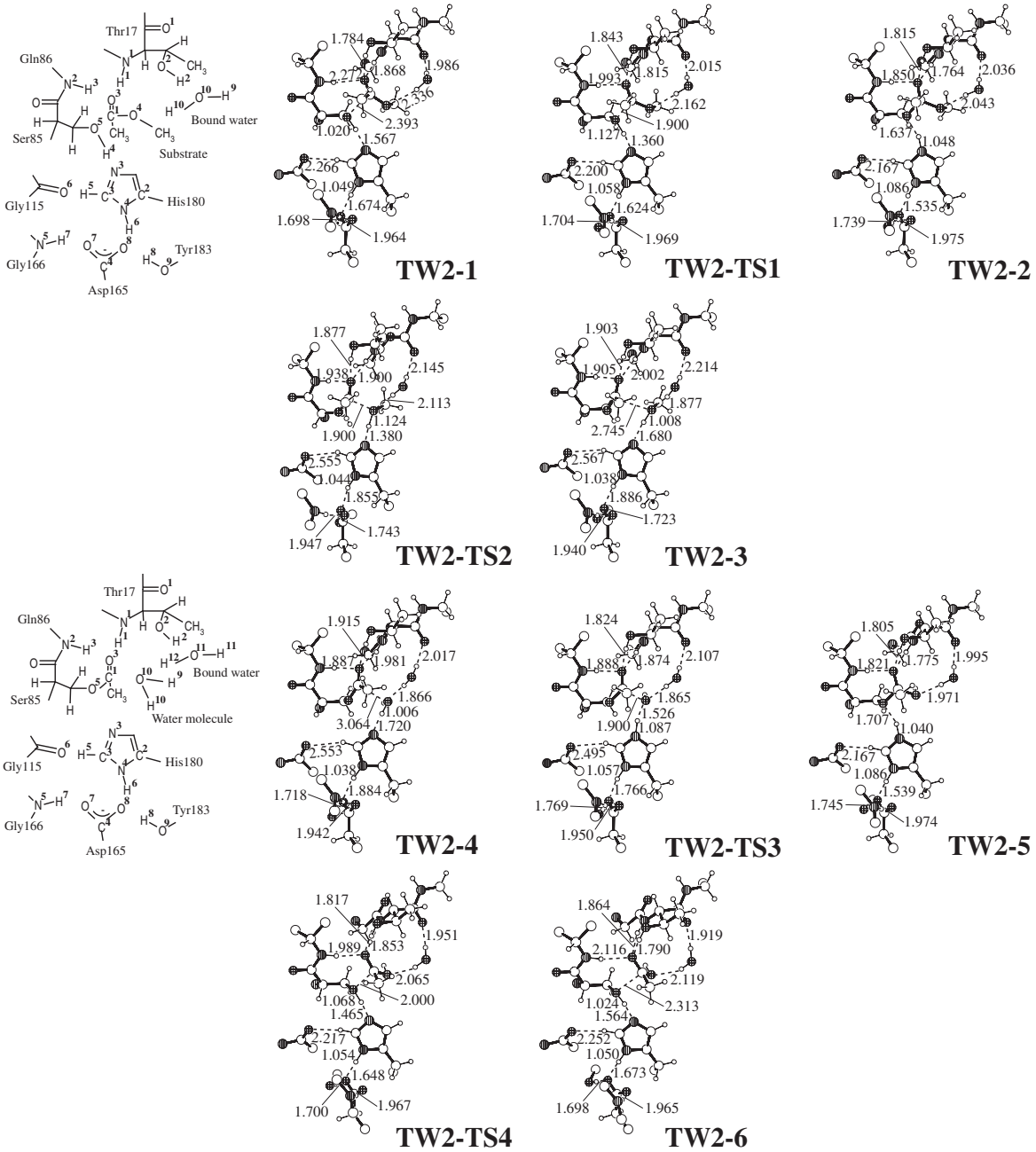

Figure 5. Optimized equilibrium and transition-state structures (in Å) involved in the catalytic cycle of the hydrolysis of biodegradable plastics by the cutinase-like enzyme (CLE) at the ONIOM(B3LYP/6-31G**:AMBER) level for Model TW2. Only the QM part is displayed for clarity.

of the hydrogens interacts with the –C–O–C– oxygen of the substrate in the transition state **TW1**–**TS1**, because the negative charge from Ser85 is delocalized in the C(–O$^-$)–O– region. The O···H(H_2O) distance shortens to 2.054 Å in the tetrahedral intermediate **TW1-2** to stabilize in energy the negatively charged substrate. The O···H(H_2O) interaction also supports the separation of the CH_3O^- in the step, **TW1-2** → **TW1-3**. In the second process, the bound water bridges Thr17 and the oxygen of the incoming H_2O. It stabilizes in energy the entire process of the nucleophilic attack of the incoming H_2O and the separation of the $CH_3C(=O)OH$ from Ser85 through the H-bond.

On the other hand, in Model TW2, although the bound water bridges Thr17 and the substrate or the incoming water, the OH hydrogen of the side chain of Thr17 interacts with the carbonyl oxygen of the substrate throughout the reaction, as presented in Figure 5. Three H-bonds of the carbonyl oxygen of the substrate with the OH of Thr17 in addition to two NH of Gln86 and Thr17 more effectively stabilize the tetrahedral intermediate **TW2-2** and **TW2-5**, as mentioned below. In addition, the bound water promotes the nucleophilic reactions in the active site through the H-bond.

Potential Energy Surfaces. The potential energy surfaces of the entire catalytic cycle from **1** to **6** at the B3LYP/6-31G**

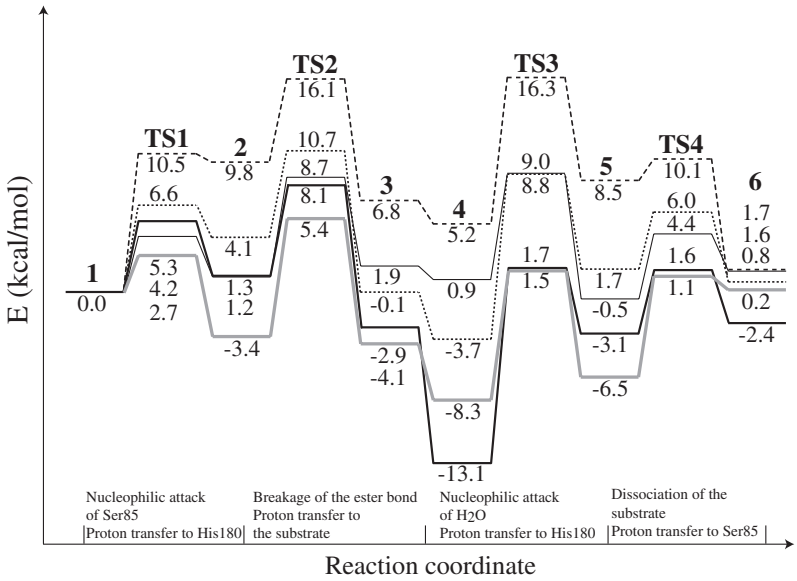

Figure 6. Potential energy surfaces of the entire catalytic cycle at the ONIOM(B3LYP/6-31G**:AMBER) level. All the energies are relative to the reactant **1**. The normal, bold, gray bold, broken, and dotted lines are for Model T, TW1, TW2, A, and AW, respectively.

level for all the models are displayed in Figure 6. The energies relative to the total energy of the fragments, which forms the intermediates and transition states involved in the catalytic reaction, are presented. In the case of Model T, both the first and second half of the catalytic reaction are almost neutral in energy. The tetrahedral intermediates, **T-2** and **T-5**, are as stable as the starting complex **T-1**, because the negatively charged carbonyl oxygen of the substrate is strongly stabilized by three H-bonds contributed by the OH group of the side chain of Thr17 in addition to the NH groups of the main chain of Thr17 and Gln86.

The energy barrier of 4.2 kcal mol^{-1} for the nucleophilic attack of Ser85 to form the tetrahedral intermediate in the step, **T-1** → **T-2**, is about half of that for the dissociation of the C–O bond of the substrate in the step, **T-2** → **T-3**, in the first half of the catalytic cycle. On the other hand, in the second half of the catalytic cycle, the energy barrier of 7.9 kcal mol^{-1} for the nucleophilic attack of the H_2O in the step, **T-4** → **T-5**, is two times larger than that for the dissociation of the C–O bond of the substrate in the step, **T-5** → **T-6**. The nucleophilicity might be larger for Ser85 than for H_2O.

The potential energy surface of Model TW1 with bound water is obviously different from that of Model T in the second process, whereas there is no significant difference between them in the first process. The energy surface of both steps of the nucleophilic attack of the H_2O and the C–O bond dissociation in the second process are much lowered by the bound water, because the bound water promotes both reactions through the H-bond. The nucleophilicity of the H_2O would be much enhanced by the bound water. The polarity of the O–H bond of the H_2O in **TW1-4** and of the C–O(H) bond of the substrate in **TW1-5** would be increased by the interaction with the bound water. These are reflected in the long O–H distance of the H_2O of 1.811 Å in **TW1**–**TS3** and in the short O–H distance of Ser85 of 1.088 Å in **TW1**–**TS4**, which are obviously different from the case of Model T. Similar trends were found in the case of Model TW2, where the bound water contributes to the reaction in the same manner, and the stability of the transition states, **TW2**–**TS3** and **TW2**–**TS4**, are as stable in energy as the transition states, **TW1**–**TS3** and **TW1**–**TS4**, respectively. In addition, since the OH group of the side chain of Thr17 interacts with the carbonyl oxygen of the substrate, both transition states, **TW2**–**TS1** and **TW2**–**TS2**, in the first half of the catalytic cycle are also stabilized by 2.6–2.7 kcal mol^{-1} compared to the corresponding transition states for Model TW1. As a result, the highest point of the rate-determining step of the C–O bond dissociation of the first half of the catalytic cycle is reduced to 5.4 kcal mol^{-1}.

We also calculated the potential energy surface for a mutant of the CLE (Model A), where Thr17 is replaced by Ala17, to clarify the effects of the OH group of the side chain of Thr17. The reaction system lacks the interaction of the OH group of the side chain with the carbonyl oxygen of the substrate throughout the reaction as presented in Figure S1. Due to the loss of this interaction, the entire potential energy surface is shifted up by 5.2–7.4 kcal mol^{-1} compared to that for Model T. On the other hand, the entire potential energy surface is shifted down by the addition of a bound water (Model AW). A bound water bridges the carbonyl oxygen of the main chain of Ala17 and the –C–O–C– oxygen of the substrate or the incoming water as presented in Figure S2. The transition state as well as the intermediate is stabilized by the H-bond of the bound water in each step. However, the entire energy surface is still higher in energy than those for Model TW1 and TW2, which indicates that the OH group of the side chain of Thr17 significantly contributes to stabilize the entire potential energy surface. As a result, Model TW2, where the OH group of the side chain of Thr17 interacts with the carbonyl oxygen of the substrate and the bound water bridges carbonyl oxygen of the main chain of Thr17 and the substrate, is the most favorable in energy. In Model TW2, the highest point of the energy surface is less than 6 kcal mol^{-1} and the rate-determining step is the C–O bond

dissociation of the substrate, **TW2-2** → **TW2–TS2** → **TW2-3**, of the first half of the catalytic reaction.

Conclusion

We theoretically examined the reaction mechanism of the cutinase-like enzyme (CLE), which degrades biodegradable plastics very efficiently, using the ONIOM method. We optimized all the intermediates and transition states involved in the catalytic cycle and determined the energy surface of the entire catalytic reaction. The calculations showed that the amino acid residues in the active site, Ser85, His180, and Asp165, which compose the catalytic triad, and Gly115, Gly166, Tyr183, Thr17, and Gln86, which stabilize the catalytic triad or the substrate, significantly contribute to the catalytic reaction. We further examined the contribution of the OH group of the side chain of Thr17 and bound water. The OH group of the side chain of Thr17 stabilizes the entire energy surface of the catalytic reaction by the formation of the H-bond with the carbonyl oxygen of the substrate. On the other hand, bound water interacts with the active site and enhances especially the nucleophilic attack of the incoming H_2O in the second process of the catalytic cycle. These electronic effects of the OH group of Thr17 and bound water are considered to be one of the factors to enhance the catalytic activity of the CLE. The calculated potential energy surface showed that the cleavage of the ester bond of the first half of the catalytic cycle is a rate-determining step.

The calculations were in part carried out at the Research Center for Computational Science (RCCS), Okazaki Research Facilities, National Institutes of Natural Sciences (NINS), Japan. This study was partly supported by grants from the Ministry of Education, Culture, Sports, Science and Technology of Japan.

Supporting Information

Figure S1: Optimized equilibrium and transition-state structures involved in the catalytic cycle for Model A. Figure S2: Optimized equilibrium and transition-state structures involved in the catalytic cycle for Model AW. This material is available free of charge on the web at http://www.csj.jp/journals/bcsj/.

References

1 K. Masaki, N. R. Kamini, H. Ikeda, H. Iefuji, *Appl. Environ. Microbiol.* **2005**, *71*, 7548.

2 D. L. Nelson, M. M. Cox, *Lehninger Principles of Biochemistry*, 3rd ed., Worth, New York, **2000**.

3 C. Branden, J. Tooze, *Introduction to Protein Structure*, 2nd ed., Newton Press, New York, **1999**.

4 G.-S. Li, B. Maigret, D. Rinaldi, M. F. Ruiz-López, *J. Comput. Chem.* **1998**, *19*, 1675.

5 C.-H. Hu, T. Brinck, K. Hult, *Int. J. Quantum Chem.* **1998**, *69*, 89.

6 E. L. Ash, J. L. Sudmeier, E. C. De Fabo, W. W. Bachovchin, *Science* **1997**, *278*, 1128.

7 F. M. L. G. Stamato, E. Longo, L. M. Yoshioka, R. C. Ferreira, *J. Theor. Biol.* **1984**, *107*, 329.

8 S. Nakagawa, H. Umeyama, T. Kudo, *Chem. Pharm. Bull.* **1980**, *28*, 1342.

9 M. W. Hunkapiller, M. D. Forgac, J. H. Richards, *Biochemistry* **1976**, *15*, 5581.

10 M. W. Hunkapiller, S. H. Smallcombe, D. R. Whitaker, J. H. Richards, *Biochemistry* **1973**, *12*, 4732.

11 J. W. Ponder, F. M. Richards, *J. Comput. Chem.* **1987**, *8*, 1016.

12 C. E. Kundrot, J. W. Ponder, F. M. Richards, *J. Comput. Chem.* **1991**, *12*, 402.

13 M. E. Hodsdon, J. W. Ponder, D. P. Cistola, *J. Mol. Biol.* **1996**, *264*, 585.

14 R. V. Pappu, R. K. Hart, J. W. Ponder, *J. Phys. Chem. B* **1998**, *102*, 9725.

15 P. Ren, J. W. Ponder, *J. Comput. Chem.* **2002**, *23*, 1497.

16 P. Ren, J. W. Ponder, *J. Phys. Chem. B* **2003**, *107*, 5933.

17 W. D. Cornell, P. Cieplak, C. I. Bayly, I. R. Gould, K. M. Merz, Jr., D. M. Ferguson, D. C. Spellmeyer, T. Fox, J. W. Caldwell, P. A. Kollman, *J. Am. Chem. Soc.* **1995**, *117*, 5179.

18 P. Kollman, R. Dixon, W. Cornell, T. Fox, C. Chipot, A. Pohorille, in *Computer Simulation of Biomolecular Systems*, ed. by W. F. van Gunsteren, P. K. Weiner, A. J. Wilkinson, Escom, Netherlands, **1997**, Vol. 3, pp. 83–96.

19 G. Moyna, H. J. Williams, R. J. Nachman, A. I. Scott, *Biopolymers* **1999**, *49*, 403.

20 W. S. Ross, C. C. Hardin, *J. Am. Chem. Soc.* **1994**, *116*, 6070.

21 J. Aqvist, *J. Phys. Chem.* **1990**, *94*, 8021.

22 F. Maseras, K. Morokuma, *J. Comput. Chem.* **1995**, *16*, 1170.

23 T. Matsubara, S. Sieber, K. Morokuma, *Int. J. Quantum Chem.* **1996**, *60*, 1101.

24 T. Matsubara, F. Maseras, N. Koga, K. Morokuma, *J. Phys. Chem.* **1996**, *100*, 2573.

25 M. Svensson, S. Humbel, R. D. J. Froese, T. Matsubara, S. Sieber, K. Morokuma, *J. Phys. Chem.* **1996**, *100*, 19357.

26 S. Dapprich, I. Komáromi, K. S. Byun, K. Morokuma, M. J. Frisch, *THEOCHEM* **1999**, *461–462*, 1.

27 T. Vreven, K. Morokuma, *J. Comput. Chem.* **2000**, *21*, 1419.

28 K. Morokuma, *Bull. Korean Chem. Soc.* **2003**, *24*, 797.

29 M. J. Frisch, G. W. Trucks, H. B. Schlegel, G. E. Scuseria, M. A. Robb, J. R. Cheeseman, J. A. Montgomery, Jr., T. Vreven, K. N. Kudin, J. C. Burant, J. M. Millam, S. S. Iyengar, J. Tomasi, V. Barone, B. Mennucci, M. Cossi, G. Scalmani, N. Rega, G. A. Petersson, H. Nakatsuji, M. Hada, M. Ehara, K. Toyota, R. Fukuda, J. Hasegawa, M. Ishida, T. Nakajima, Y. Honda, O. Kitao, H. Nakai, M. Klene, X. Li, J. E. Knox, H. P. Hratchian, J. B. Cross, V. Bakken, C. Adamo, J. Jaramillo, R. Gomperts, R. E. Stratmann, O. Yazyev, A. J. Austin, R. Cammi, C. Pomelli, J. W. Ochterski, P. Y. Ayala, K. Morokuma, G. A. Voth, P. Salvador, J. J. Dannenberg, V. G. Zakrzewski, S. Dapprich, A. D. Daniels, M. C. Strain, O. Farkas, D. K. Malick, A. D. Rabuck, K. Raghavachari, J. B. Foresman, J. V. Ortiz, Q. Cui, A. G. Baboul, S. Clifford, J. Cioslowski, B. B. Stefanov, G. Liu, A. Liashenko, P. Piskorz, I. Komaromi, R. L. Martin, D. J. Fox, T. Keith, M. A. Al-Laham, C. Y. Peng, A. Nanayakkara, M. Challacombe, P. M. W. Gill, B. Johnson, W. Chen, M. W. Wong, C. Gonzalez, J. A. Pople, *Gaussian 03*, Gaussian, Inc., Wallingford CT, **2004**.

30 C. Lee, W. Yang, R. G. Parr, *Phys. Rev. B* **1988**, *37*, 785.

31 A. D. Becke, *J. Chem. Phys.* **1993**, *98*, 5648.

32 J. Wang, R. M. Wolf, J. W. Caldwell, P. A. Kollman, D. A. Case, *J. Comput. Chem.* **2004**, *25*, 1157.

33 S. N. Rao, U. C. Singh, P. A. Bash, P. A. Kollman, *Nature* **1987**, *328*, 551.

34 S. Braxton, J. A. Wells, *J. Biol. Chem.* **1991**, *266*, 11797.
35 Z. S. Derewenda, U. Derewnda, P. M. Kobos, *J. Mol. Biol.* **1994**, *241*, 83.
36 E. L. Ash, J. L. Sudmeier, R. M. Day, M. Vincent, E. V. Torchilin, K. C. Haddad, E. M. Bradshaw, D. G. Sanford, W. W. Bachovchin *Proc. Natl. Acad. Sci. U.S.A.* **2000**, *97*, 10371.
37 M. Topf, P. Várnai, G. Richards, *J. Am. Chem. Soc.* **2002**, *124*, 14780.
38 T. Ishida, *Biochemistry* **2006**, *45*, 5413.